Radiation Physics and Chemistry 155 (2019) 184–190

Contents lists available at ScienceDirect

Radiation Physics and Chemistry

journal homepage: www.elsevier.com/locate/radphyschem

Fast-neutron detector developments for the TREAT hodoscope

Jeremy A. Roberts*, Mark J. Harrison, Wenkai Fu, Priyarshini Ghosh, Douglas S. McGregor

Department of Mechanical and Nuclear Engineering, Kansas State University, Manhattan, KS 66506, USA

ARTICLE INFO

Keywords:
Fast-neutron detection
Hodoscope
Hornyak button
Microstructured neutron detector
TREAT

ABSTRACT

This work describes the theoretical and experimental performances of four alternatives to the original Hornyak Button-type device that was used in the construction of the Transient Reactor Test (TREAT) Facility hodoscope. The alternatives considered differ in geometry, construction and detection materials to improve performance while decreasing some of the negative aspects of the original device. A Geant4 model of the original Hornyak Button was developed as a benchmark to validate the physics modeled, which agreed well with the reported values. The four alternatives considered were (1) a homogenized ZnS:Ag/PMMA rectangular bar outfitted with silicon photomultipliers (SiPMs), (2) a layered ZnS:Ag/PMMA rectangular bar detector also outfitted with SiPMs, (3) a microstructured neutron detector (MSND) backfilled with hydrogenous material and (4) a pressurized, organic gaseous scintillator. In two scintillation devices, SiPMs were considered as a replacement for photomultiplier tubes for greater light collection. These alternatives were considered as they each had the potential to provide better signal-to-noise ratios, reduce Čerenkov light production, increase detection efficiency, and/or improve neutron-to-gamma discrimination. At comparable lengths, the layered design has been experimentally determined to yield an efficiency of 1.3% (the Hornyak button exhibits 0.4%), while studies on the performances of the other detectors are still underway.

1. Introduction

The Transient Reactor Test (TREAT) Facility at Idaho National Laboratory (INL) was designed for testing materials under a variety of transient conditions that simulate real-world, accident scenarios. The reactor is air cooled and fueled with uranium-filled, graphite blocks that can be arranged in a core with a central, voided slot. Test specimens are placed in this slot, which is in line with a fast-neutron hodoscope that images specimen motion by detecting neutrons emerging from fission within the specimen. The TREAT hodoscope has a thick conical front collimator, a large bank of diverging collimators, beyond which are thick plates of lead shielding, and finally slots for individual neutron detectors. The collimator bank is formed from 10 columns and 36 rows. The detector slots are approximately 1 in. diameter. An illustrative schematic of the hodoscope is shown in Fig. 1.

The hodoscope in past experiments was outfitted with Hornyak button-type devices as fast neutron detectors, each with an individual photomultiplier tube, and provided time and spatial resolution of fuel motion during reactor power transient experiments. It also provided information on nuclear fuel displacements and changes before, during, and after a transient experiment. Additional detectors used included methane-filled, proportional counters (DeVolpi, 1989) and fission chambers (De Volpi, 1975) for neutrons and NaI detectors for gamma rays (DeVolpi, 1989). Although the Hornyak buttons were historically the primary neutron detectors (De Volpi et al., 1975) and are presently the detectors of interest for refurbishment and replacement efforts, the alternative neutron detectors provided back-up measurements for all tests and, with their lower efficiency, were better able to provide linear responses during transient peaks. For such transients, an additional lead filter was situated between the collimator exit and the detector arrays in order to reduce gamma-ray induced pileup in the Hornyak buttons (De Volpi, 1975).

With the recent restart of the TREAT facility, the detectors for the hodoscope are in need of replacement. Described are four alternative detectors under investigation as potential replacements for the older Hornyak buttons previously used.

2. Methods

2.1. Hornyak-button

The Hornyak button, as used previously in the TREAT hodoscope, consisted of a $2.8 \times 15.9 \times 25.4\ mm^3$ central active rectangular slab and optically coupled half-cylinder PMMA (Lucite) light guides, as shown in Fig. 2. The slab is a mixture of 5% mass ratio ZnS:Ag in the PMMA. Fast neutrons can interact with the hydrogen in the detector to generate

* Corresponding author.
E-mail address: jaroberts@ksu.edu (J.A. Roberts).

https://doi.org/10.1016/j.radphyschem.2018.06.008
Received 21 October 2017; Received in revised form 4 June 2018; Accepted 7 June 2018
Available online 15 June 2018
0969-806X/

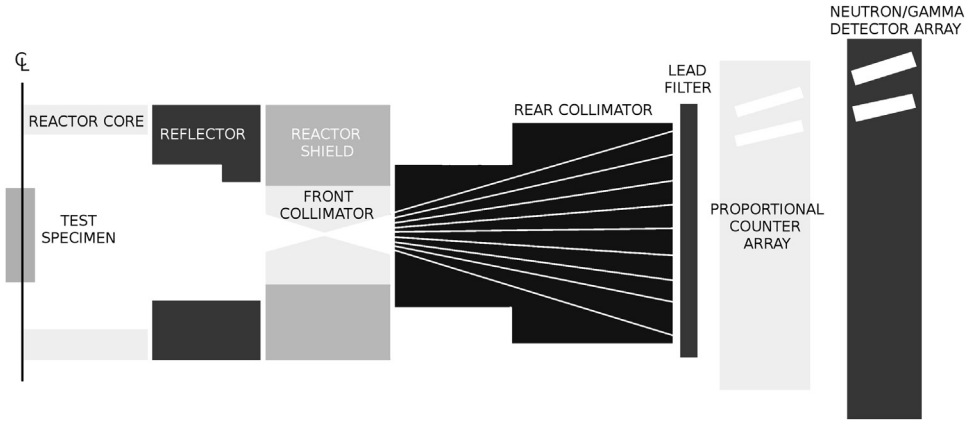

Fig. 1. Schematic of the Hornyak button fast neutron detector. (After Rhodes et al., 1992).

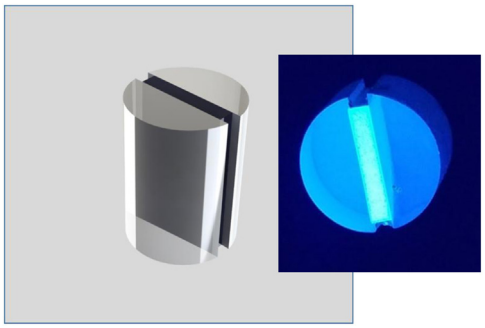

Fig. 2. Schematic of the Hornyak button fast neutron detector.

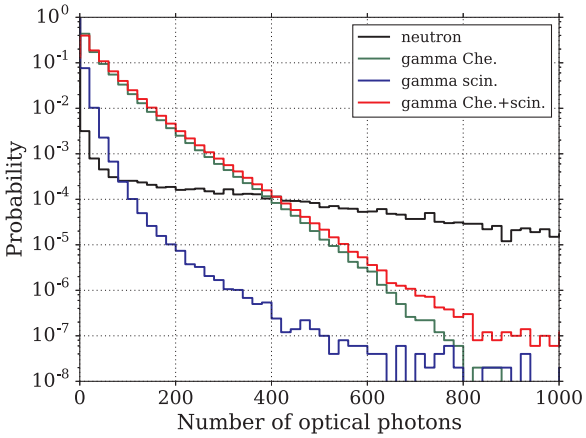

Fig. 3. The simulated neutron and gamma-ray spectra of the Hornyak button model.

recoil protons. If the recoil protons deposit energy in the suspended scintillating ZnS:Ag particles, light is emitted. The light can then be shuttled to the photomultiplier tube (PMT) by the light guides to generate detectable pulses. Under ideal conditions, the Hornyak button has an efficiency of about 0.4% for fast neutrons, with good rejection of about 10^{-8} counts per incident gamma rays (De Volpi et al., 1975). However, the Hornyak button suffered from the gamma-ray induced Čerenkov noise, which was mainly generated in the PMMA (De Volpi et al., 1975). Although a pulse-shaping technique was designed to reject the Čerenkov noise, the detection system became complicated (De Volpi et al., 1975).

A model of the Hornyak button as designed for the TREAT hodoscope was constructed in Geant4 (Agostinelli et al., 2003) for a performance evaluation and benchmark, where the calculation included nuclear and optical physics. The Hornyak button was irradiated by mono-directional neutrons (one per pulse) and isotropic gamma rays (10 per neutron), with energies drawn from the appropriate energy spectra. The sampled radiation resembled the TREAT hodoscope environment. In the gamma-ray case, light generated by scintillation, Čerenkov radiation, and the combination were considered. A calculated pulse-height distribution is shown in Fig. 3, where the strong gamma-ray induced Čerenkov noise is identified. A typical origin of the Čerenkov noise is from the PMMA light guide, designed for good light-collection efficiency (De Volpi et al., 1975). A lower-level discriminator (LLD) setting at 200 optical photons can yield a neutron-detection efficiency of 0.35% while rejecting a majority of the gamma-ray scintillation light (assuming the Čerenkov noise is rejected by the pulse-shaping technique (De Volpi et al., 1975)). Hence, the computed results agreed relatively well with the reported values.

2.2. Advanced ZnS:Ag devices

Using a SiPM and/or altering the scintillation-volume configuration, two advanced ZnS:Ag detectors were considered, named the (1) layered detector and the (2) homogenized detector. Unlike the Hornyak button, where the PMT is connected to the active slab at the end, the SiPMs surround the periphery of the scintillation volumes, which eliminate the light guides to reduce the Čerenkov noise in the two new detectors. The periphery SiPMs also allow a larger length of the scintillation volumes for better efficiencies (Fig. 4).

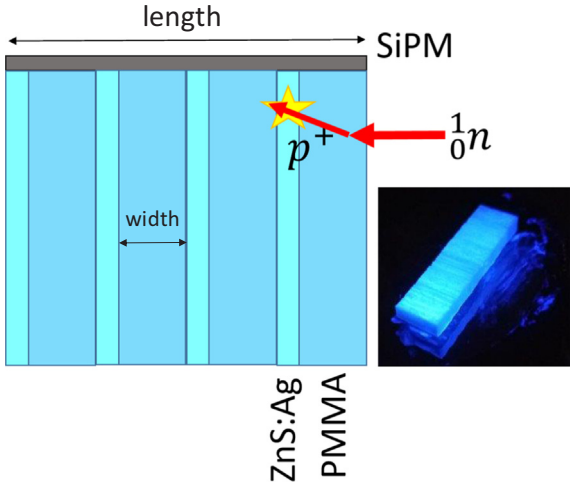

Fig. 4. Schematic of the layered detector.

Table 1
The neutron-detection efficiencies (%) of the 5-cm long, layered detectors under different layer thicknesses with sufficient LLD settings.

	ZnS(Ag) (μm)						
PMMA (mm)	2	4	7	12	21	35	59
0.10	2.05	3.02	3.15	2.49	2.21		
0.18	2.44	3.03	3.26	3.31	2.71	2.06	
0.32		2.16	2.47	2.54	2.61	2.43	2.11

2.2.1. Layered detector

For the layered detector, the scintillation volume consists of periodically alternating PMMA and ZnS:Ag layers, as shown in Fig. 4. This configuration is efficient for the preferentially forward-scattered recoil protons depositing energy in the ZnS:Ag layer, and the multiple ZnS:Ag layers can absorb a majority of the Čerenkov light in its forward-directional path. The PMMA layers provide absorption-free lateral paths for the scintillation photons.

The thicknesses of the PMMA and the ZnS:Ag layers affect the performance of the layered detector. Effects of these two parameters were evaluated in Geant4. Detectors with 5-cm length were irradiated in the same simulated environment as the Hornyak button model. Table 1 summarizes the considered PMMA and ZnS(Ag) layer thicknesses that can yield neutron-detection efficiencies above 2%. The LLDs were set to achieve a signal-to-noise (S/N) ratio of 100 considering the gamma-induced Čerenkov and scintillation noises. For the PMMA layer and the ZnS:Ag layer thicknesses of 180 μm and 12 μm, respectively, efficiency of about 3.31% can be achieved in a 5-cm long device.

Fig. 5 shows the variation of the neutron-detection efficiencies and the associated S/N ratios under different LLD settings. The detector simulated has the optimized trench-wall widths and 5-cm length. Good S/N ratios can be maintained with desirable detection efficiency.

Assuming the optimized trench-wall widths, the layered detectors' efficiencies under different lengths were evaluated. As shown in Fig. 6, the efficiency scales well with length and saturates at about 6%.

A prototype layered detector with length of 2.6 cm was made. Performance of the layered detector was compared to the original Hornyak button. Both detectors were irradiated by a ^{252}Cf source. The measurement results are shown in Fig. 7. A promising efficiency of about 1.3% was observed from the layered detector.

2.2.2. Homogenized detector

A homogenized detector is a variant of a Hornyak button (Hornyak, 1952). This design differs from the original Hornyak button deployed in the TREAT hodoscope by two main features. First, the light is collected with SiPMs attached to the Hornyak button sides rather than with a PMT attached at the back end face of the button (De Volpi et al., 1975). Second, the scintillating ZnS:Ag material is dispersed as particles within the transparent polymer rather than a single solid sliver of ZnS:Ag positioned between two PMMA half-discs (see Fig. 2). The shortened light path permits a larger concentration of ZnS:Ag component in the total volume, i.e., enhancing light yield and thus enabling lower energy scatters to be detected, improving detection efficiency. For a 5-cm homogenized detector, calculations indicate an optimal efficiency of about 1.3% at a ZnS:Ag mass ratio of approximately 13%, as shown in Fig. 8. For comparison, a 5-cm homogenized device with a ZnS:Ag mass ratio of 5% has a calculated efficiency of approximately 0.7%, twice that predicted for the 2.54-cm Hornyak-button. Performance of the 5-cm long homogenized detector with the optimized ZnS:Ag mass ratio of 13% is shown in Fig. 9.

In the laboratory, ZnS:Ag was synthesized by adding appropriate concentrations of 0.2 M $ZnSO_4$, 0.6 M $SC(NH_2)_2$, NH_4OH, $AgNO_3$ and deionized water. The resulting gelatinous concentrate was subsequently heated to 1200 ° C in a quartz tube to evaporate the water out of the paste and to activate the Ag. White ZnS:Ag was obtained in powder-form, which fluoresced a bluish purple color under deep UV irradiation, emitting a wavelength at approximately 450 nm, indicating significant (≤ 2%) dopant concentrations of Ag.

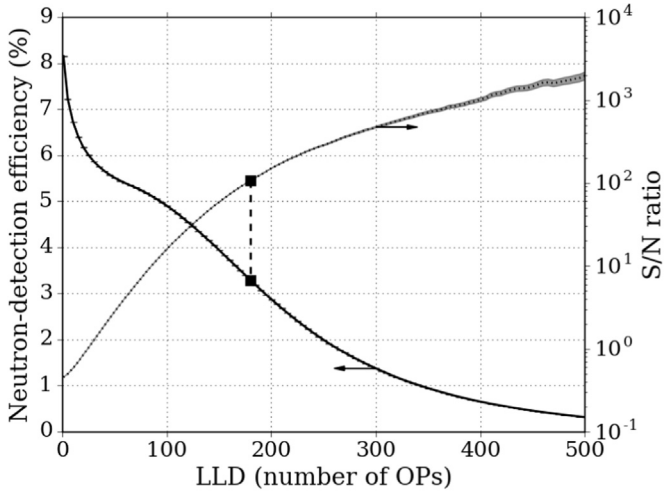

Fig. 5. The computed neutron-detection efficiencies and the corresponding S/N ratios of the 5-cm long layer detector under different LLD settings. The layer thicknesses were optimized.

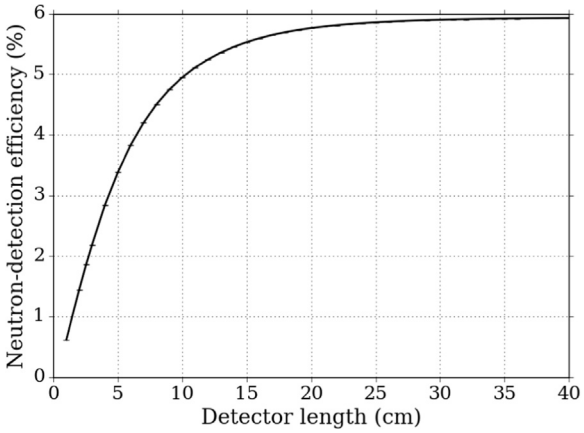

Fig. 6. The computed neutron-detection efficiencies of the layered detectors with different lengths. The layer thicknesses were optimized.

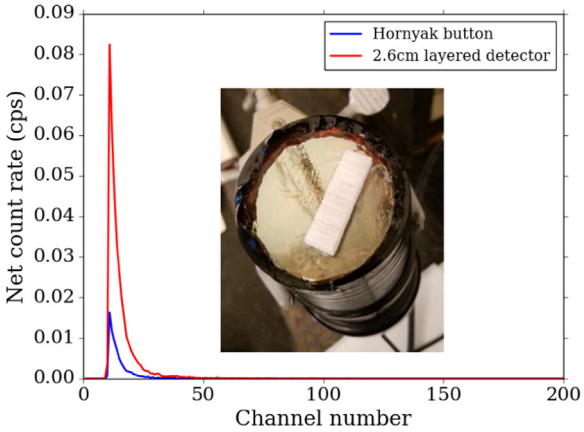

Fig. 7. The measured spectra of the prototype layered detector and the original Hornyak-like button exposed to unshielded ^{252}Cf source.

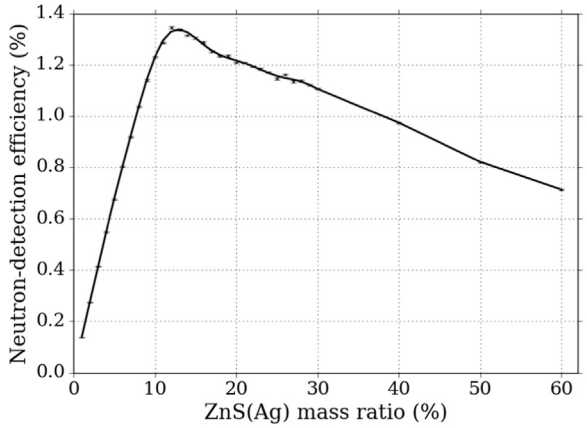

Fig. 8. The simulated neutron-detection efficiencies of the 5-cm long homogenized detectors with different ZnS:Ag concentrations.

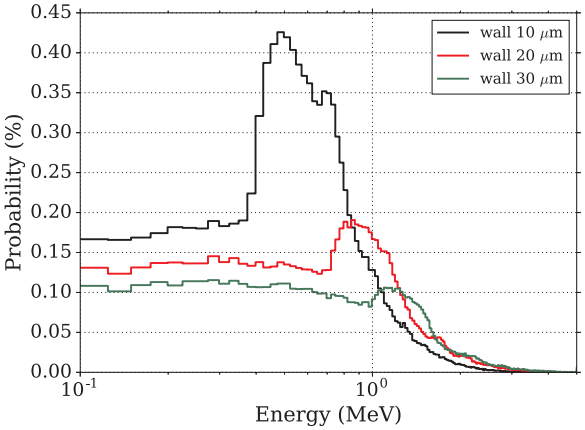

Fig. 10. The MCNP predicted neutron spectra of the 2-cm long H-MSNDs with 20-μm trench.

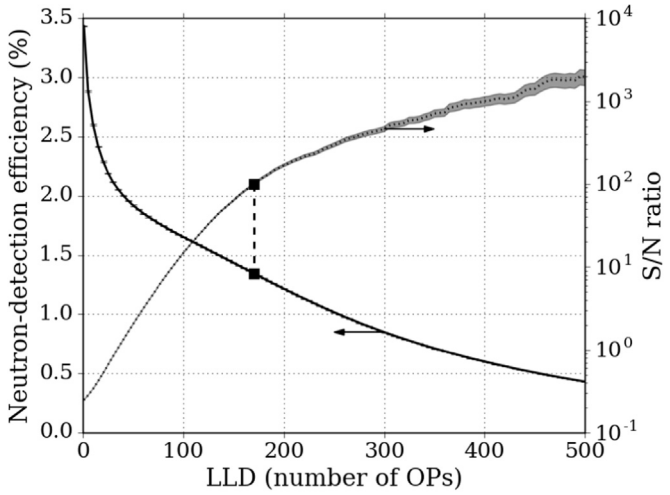

Fig. 9. The computed neutron-detection efficiencies and the associated S/N ratios under different LLD settings of the homogenized detector with the optimized ZnS:Ag mass ratio of 13%.

2.3. Hydrogenous micro-structured neutron detectors

Microstructured semiconductor neutron detectors (MSND) have deep etched features penetrating into a semiconductor surface. This surface is processed to produce a pn junction about the etched features, and a neutron reactive material is backfilled into the trenches. The most successful devices of this type are backfilled with ^{6}LiF and are designed mainly for thermal neutron detection (Bellinger et al., 2012). Neutrons absorbed in the ^{6}Li release energetic charged-particle reaction products subsequently detected in the adjacent semiconductor diode walls. For application to fast-neutron detection, actinide-filled MSNDs were considered (Ghosh et al., 2016). The predicted efficiencies were modest (up to 3% using several devices) compared to those predicted for the ZnS:Ag devices already described. Moreover, the acquisition and handling of candidate actinides (e.g., ^{237}Np, with its low thermal-neutron sensitivity) presents several logistical challenges. As an alternative, a variant of the MSND design was explored here using hydrogenous backfill material with proton recoil as the neutron reaction.

2.3.1. MCNP calculation

By replacing the reactive material ^{6}LiF (Bellinger et al., 2012) with paraffin wax, a fast-sensitive hydrogenous micro-structured semiconductor neutron detector (H-MSND) was developed. MCNP (Goorley et al., 2012) simulated pulse-height distributions of the 2-cm H-MSNDs under fission spectrum neutron irradiation are shown in Fig. 10, where the trench thickness is 20 μm. As wall thickness is increased, the spectral peak moves to higher-energy regions, which allows for a higher LLD setting. The spectral shift is a consequence of the proton recoil range and linear energy transfer (LET). For a 300-keV proton, the projected range in silicon is 3.02 μm and for a 700-keV proton, this range is 9.67 μm (Ziegler et al., 2010).

A higher LLD setting will work to reject a larger percentage of gamma rays, the major background component in the TREAT hodoscope environment (De Volpi et al., 1975). At an LLD setting at 300 keV, the 10-μm wall H-MSND is predicted to have an efficiency of about 9.8%. If the LLD setting is moved to 700 keV, the 20-μm wall H-MSND yields a calculated efficiency of approximate 5.4%. For higher efficiency, a 10-cm long H-MSND with 20-μm trench and 20-μm wall thicknesses can yield an efficiency of 14.2% at the LLD setting of 700 keV. However, for this 10-cm long H-MSND, there is a 0.87% possibility for a fission spectrum gamma photon to be detected with a 700-keV equivalent LLD setting, i.e., a S/N ratio of about 16 according to the simulation. Experimentally, the gamma sensitivity of the H-MSND was found to be problematic. Hence, further optimization for better S/N ratio is necessary.

2.3.2. Experimental procedure

Several standard 1.0 × 1.0 cm^2 MSND diodes were heated above the melting point of paraffin wax with the top of the trenches being cooler than the bottom of the diode, small chips of paraffin wax were carefully placed on top of the diodes and allowed to melt into the trenches. The established temperature gradient preferentially pulled the molten wax down into the trenches. Once entirely filled, the diodes were removed from the heat source and allowed to cool. The wax hardened and any remaining paraffin wax at the top of the diodes was scraped off to yield well-filled trenches with minimal wax above the trenches. Fig. 11 is a scanning electron microscope image of a cross-section of the MSND trenches, showing good filling behavior.

2.3.3. Measurement

The constructed prototype H-MSND devices were then experimentally investigated for neutron and gamma sensitivity. Basic laboratory measurements indicated the H-MSNDs were more sensitive to gamma-rays than expected, prompting an investigation into their behavior in a scenario more closely resembling the devices' intended application by making measurements at the fast-beam port of the TRIGA Mark II nuclear reactor at Kansas State University. An unfilled MSND fabricated in the same batch as the prototype H-MSND diodes was also measured. The difference between the unfilled and filled devices directly identified the impact of the paraffin wax backfill in the device's radiation sensitivity. Fig. 12 shows the measured spectra of the paraffin wax filled MSND and the blank MSND. As shown in Fig. 12, the overall count rates

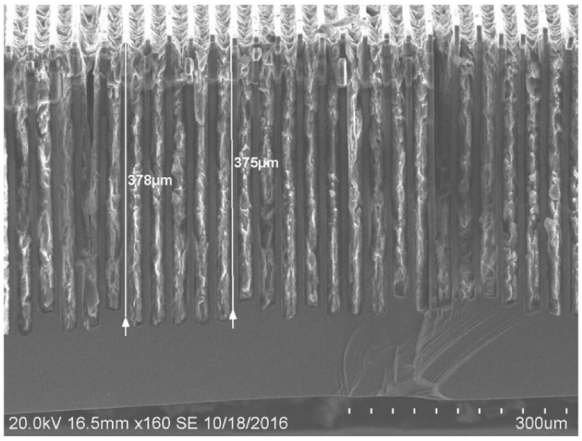

Fig. 11. The fabricated MSND filled with paraffin wax.

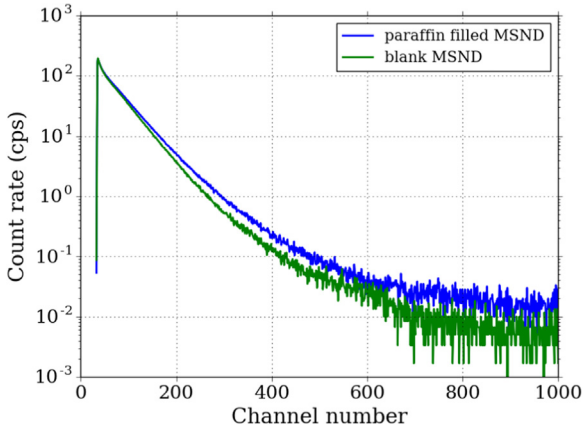

Fig. 12. The measured spectra of the paraffin wax filled MSND and the blank MSND at the beam port of the TRIGA Mark II nuclear reactor at Kansas State University.

for both devices were high, but with little difference between them. This indicates that a preponderance of the counts recorded were due to the gamma-rays, not neutrons, since the blank MSND would be largely insensitive to neutrons.

Plotted in Fig. 13 are the difference spectrum between the two devices (blank and paraffin-filled) and the S/N ratio. Here, the S/N ratio was computed as the ratio between the net count rate and blank MSND count rate, and afterwards smoothed. It can be noted in Fig. 13 the S/N ratio does not reach 1:1 until approximately channel 700 and never achieves a 10:1 ratio.

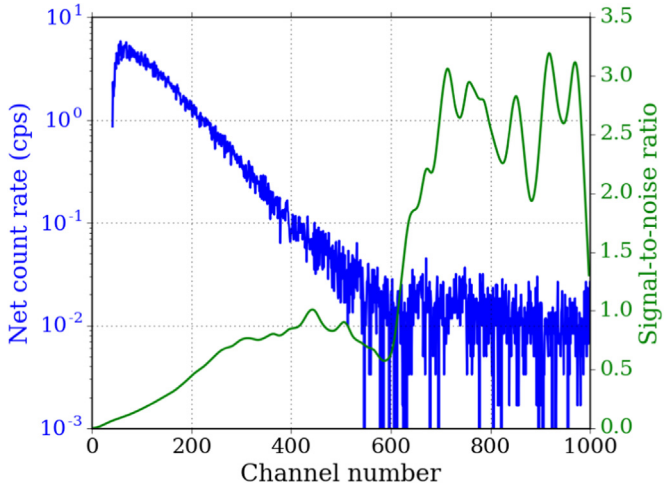

Fig. 13. The net count rates and the associated S/N ratios under different LLD settings based on the measured results of the two MSND devices.

2.4. Pressurized organic gas scintillator

2.4.1. MCNP calculation

Gaseous scintillators, sensitized to fast neutrons by incorporation of hydrogen in the gas mixture, present a promising candidate technology for the hodoscope application from a number of aspects. First, they can be constructed such that their composition is low effective Z and low mass density, so that gamma-ray contamination is minimized. Second, the effective index of refraction in the gas is nearly unity (approx. 1.0005) thereby minimizing Čerenkov contamination as well.

A gas scintillation detector was simulated consisting of a mixture of hydrogen and tetrafluoromethane (CF_4) gas under a total of 3-atm pressure, enclosed in a 10 cm long cylinder with diameter 2.87 cm. The hydrogen concentration of the gas was varied to determine its effect on detection efficiency.

A fast neutron in this device is detected via scintillation light emitted by CF_4. Because the increase of hydrogen concentration decreases the density of the mixture, the impact of mass fraction of hydrogen gas on the detection efficiency was evaluated in MCNP. The detector was irradiated by fission-spectrum neutrons incident on the detector face in the longitudinal direction. Assuming their deposited energy by proton recoil contributed to the scintillation process, and applying a LLD at 300 keV, the detection efficiency as a function of the hydrogen concentration is shown in Fig. 14, which indicates a 50 wt% hydrogen concentration can yield a best efficiency of about 3.5%. These computational results, of course, assumed the energy transfer mechanism from the recoil protons to the CF_4 gas molecules is efficient. It was found experimentally, though, that this energy transfer is inefficient and deleterious to detection efficiency.

2.4.2. Emission spectrum of CF_4 gas

Shown in Fig. 15 is the emission spectrum of the CF_4 gas. The spectrum features a peak near 295 nm with broad spread. The spectrum does not couple well to traditional PMTs. However, newer multi-alkali photocathode PMTs can achieve integral quantum efficiencies on the order of about 20%.

2.4.3. Alpha particle response

A prototype was built to determine the light intensity with respect to gas composition, as shown in Fig. 16. Different gas compositions were tested using an alpha particle source. Shown in Fig. 17 are measured spectra of the CF_4 gas under different pressures. The CF_4 gas at

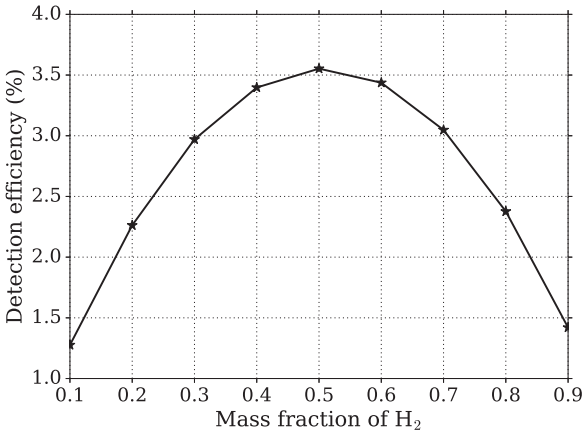

Fig. 14. The MCNP-computed efficiencies of the scintillation gas detectors with different hydrogen concentrations.

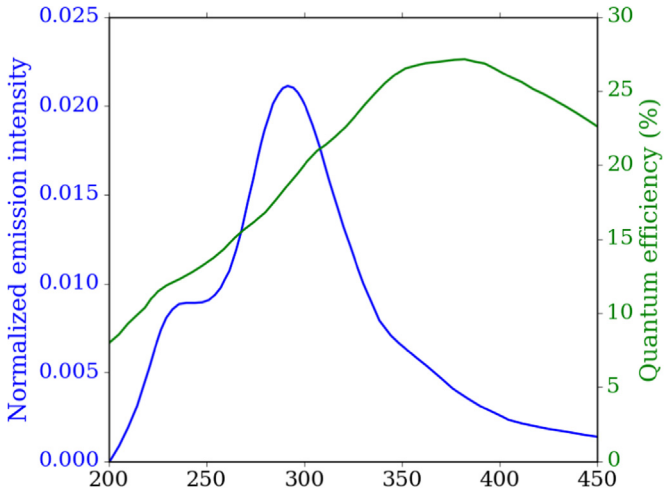

Fig. 15. The emission spectrum of the CF_4 gas and the quantum efficiency curve of the Hamamatsu R750 PMT used in the experiment.

the pressure of 2.4 atm has the strongest light intensity, indicating that there is an optimal gas pressure of CF_4 for highest light yield. In other words, light yield decreased for gas pressures greater than or less than this observed optimum.

Introducing H_2 to the CF_4 added significant complexity as the effect of the H_2 on the scintillation of CF_4 had to be determined. The measured alpha-particle spectra under different H_2 concentrations are shown in Fig. 18. Most notable is the fact that the higher channel counts present in the pure CF_4 spectrum are absent in all spectra from H_2-containing spectra. This indicates a loss of energy transfer to the CF_4 molecules and/or a decrease in the light signal from the CF_4 molecules to the PMT.

2.4.4. Neutron response

While the alpha spectra provided insight into the energy transfer process, ultimately the device should provide good neutron detection characteristics. As such, the investigation proceeded by irradiating the device with a ^{252}Cf source while gas composition and pressures were varied. First, a measurement of the chamber filled with 1.01 atm of CF_4 and varying amounts of H_2 was performed. Results are shown in Fig. 19, where it can be observed that the addition of H_2 to the chamber actually degraded neutron detection efficiency.

To further prove this phenomenon, an additional ^{252}Cf measurement was performed. The first measurement configuration was for 0.0072-mol CF_4 mixed with 0.0239-mol H_2. Next, the H_2 content was increased (approximately doubled) to 0.0481-mol H_2, while keeping the CF_4 content constant. The third and final measurement was for a mixture with approximately double the CF_4 content as the first two (0.015-mol vs 0.0072-mol) and 70% the H_2 content as the first

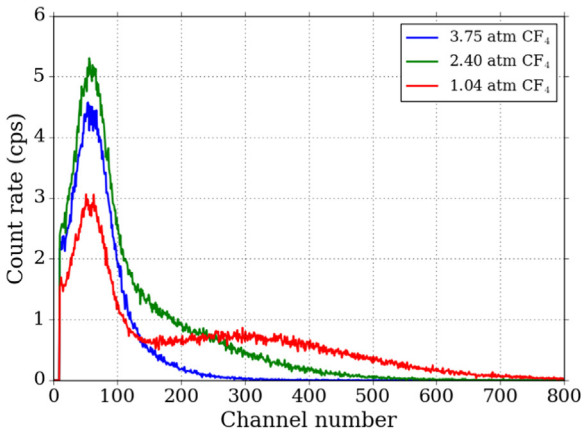

Fig. 17. The measured alpha spectra of pure CF_4 gas with different pressures.

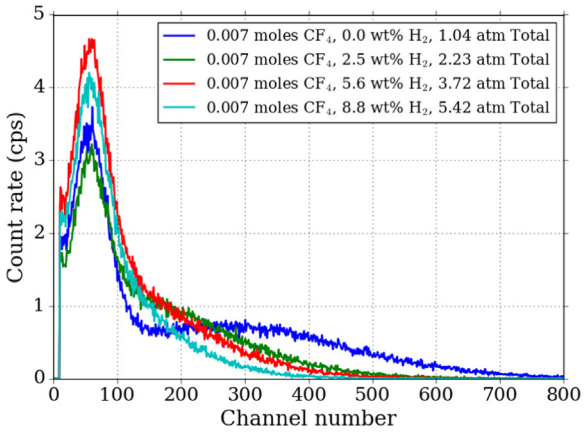

Fig. 18. The measured alpha spectra of 0.007 moles CF_4 gas with different hydrogen contents and total pressures.

measurement (0.0160-mol vs 0.0239-mol). Shown in Fig. 20 are the results of this series of measurements. Increasing the H_2 content reduced detection efficiency while increasing CF_4 content increased efficiency proportionally. These results clearly indicate that the addition of H_2 to the mixture is deleterious to the detection process.

2.5. Conclusion

The investigation of four alternative technologies to replace the previously-used Hornyak-type devices in the TREAT hodoscope produced at least one promising candidate, the layered ZnS:Ag/PMMA device. There are manufacture and reproducibility concerns regarding the homogenized ZnS:Ag/PMMA device, mainly because ZnS:Ag is

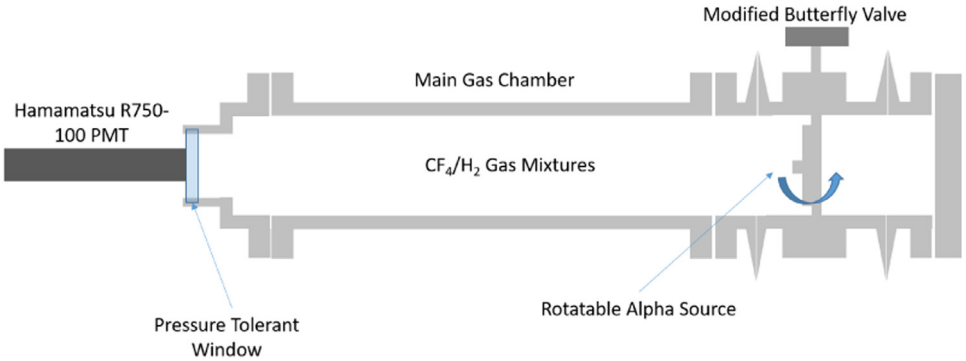

Fig. 16. Schematic of the constructed prototype to measure the light intensity of different gas compositions.

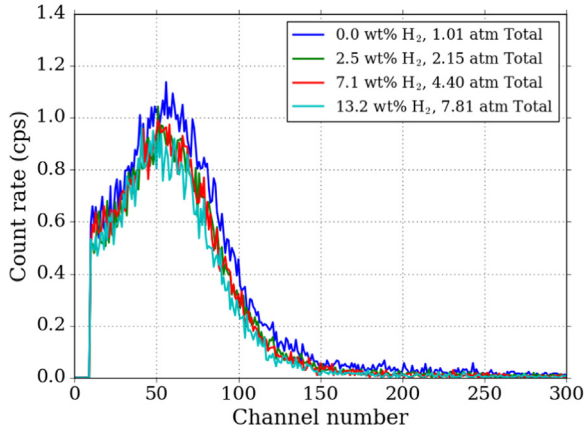

Fig. 19. The measured neutron spectra of the gas detectors under different hydrogen concentrations. The CF_4 content was 0.0072 moles in all the cases.

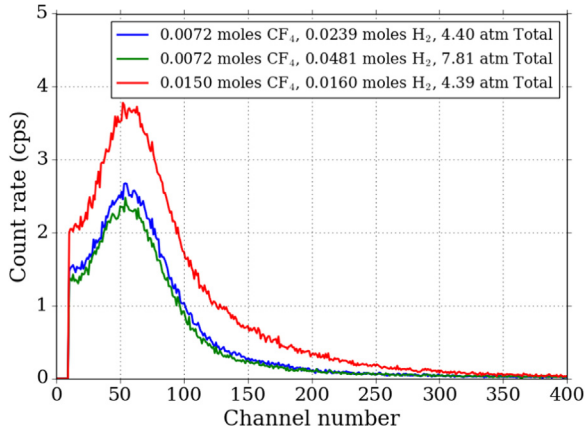

Fig. 20. The measured ^{252}Cf spectra with respect to varied CF_4 and H_2 contents and total pressures.

insoluble in PMMA, thereby, making the suspension of ZnS:Ag in PMMA non-uniform. Coupling these issues with the lower (predicted) maximum detection efficiency, the homogenized ZnS:Ag/ PMMA device appears less attractive than the layered device. For the H-MSND and the gaseous organic scintillator, production is simple. However, the H-MSND suffers from other concerning features. Namely, the H-MSND has a poor S/N ratio due to its gamma-ray sensitivity. The gaseous organic scintillator remains a viable candidate as it is predicted to be capable of achieving 1.3% efficiency without the addition of H_2 and, of course, has minimal Čerenkov contamination. Of the four detector constructions tested, the layered ZnS:Ag/PMMA device has proven to be both easily manufactured and achieves significant efficiency improvements for a 2.6-cm long device. Models indicate considerable efficiency improvements can be realized for the layered ZnS:Ag/PMMA detector if the length is increased.

Acknowledgements

This material is based upon work supported by the U.S. Department of Energy, Office of Nuclear Energy under Award no. DE-NE0008305.

References

Agostinelli, S., Allison, J., Amako, K., Apostolakis, J., Araujo, H., Arce, P., Asai, M., Axen, D., Banerjee, S., Barrand, G., et al., 2003. Geant4 – a simulation toolkit. Nucl. Instrum. Methods Phys. Res. Sect. A 506 (3), 250–303.

Bellinger, S., Fronk, R., Sobering, T., McGregor, D., 2012. High-efficiency microstructured semiconductor neutron detectors that are arrayed, dual-integrated, and stacked. Appl. Radiat. Isot. 70 (7), 1121–1124.

De Volpi, A., Pecina, R., Daly, R., Travis, D., Stewart, R., Rhodes, E., 1975. Fast-neutron hodoscope at TREAT: development and operation. Nucl. Technol. 27 (3), 449–487.

De Volpi, A., 1975. Current developments in treat hodoscope technology. In: Proceedings of the Trans. Information Exchange Conference on Reactor Fuel and Clad Motion Diagnostics. Albuquerque, NM.

DeVolpi, A., 1989. Neutron-Gamma Hodoscope Detection of Fissile Materials.

Ghosh, P., Fu, W., Fronk, R., McGregor, D., Roberts, J., 2016. Evaluation of msnds for fast-neutron detection and the treat hodoscope. Trans. Am. Nucl. Soc. 115, 1009–1012.

Goorley, T., James, M., Booth, T., Brown, F., Bull, J., Cox, L., Durkee, J., Elson, J., Fensin, M., Forster, R., et al., 2012. Initial MCNP6 release overview. Nucl. Technol. 180 (3), 298–315.

Hornyak, W., 1952. A fast neutron detector. Rev. Sci. Instrum. 23 (6), 264–267.

Rhodes, E., Bauer, T., Stanford, G., Regis, J., Dickerman, C., 1992. Fuel motion in over-power tests of metallic integral fast reactor fuel. Nucl. Technol. 98 (1), 91–99.

Ziegler, J.F., Ziegler, M.D., Biersack, J.P., 2010. SRIM-the stopping and range of ions in matter (2010). Nucl. Instrum. Methods Phys. Res. Sect. B: Beam Interact. Mater. At. 268 (11), 1818–1823.